Acta Cryst. (1977). A33, 90–97

Simultaneous Four-Beam Borrmann Diffraction*

BY BEN POST, S. L. CHANG† AND T. C. HUANG‡

Physics Department, Polytechnic Institute, Brooklyn, New York 11201, *USA*

(*Received* 23 *April* 1976; *accepted* 19 *July* 1976)

A general procedure is described for the calculation of *n*-beam Borrmann diffraction effects. These include the coordinates of points on the sheets of the dispersion surface, absorption coefficients, excitation of modes of propagation and transmitted intensities. The procedure has been used to calculate four-beam effects involved in the simultaneous transmission of the 000, $1\bar{1}1$, $3\bar{1}\bar{1}$ and $20\bar{2}$ reflections through essentially perfect germanium crystals. Emphasis has been placed on calculations which illustrate the transitions from four-beam interactions to one or two-beam cases. The minimum value of the absorption coefficients for Cu $K\alpha_1$ at the exact four-beam setting is 6·2 cm^{-1}, compared with the 'normal' coefficient of 352 cm^{-1}. The effects of several relevant variables on transmitted intensities and on the effective absorption coefficients, are described. High-resolution divergent-beam photographs, utilizing a microbeam X-ray source and an evacuated path of 160 cm from crystal to film, reveal a number of previously unreported anomalies in the transmitted intensities. The calculated values of the corresponding reflection intensities agree well with these observations.

1. Introduction

When an unpolarized, monochromatic beam of X-rays is incident on the surface of a perfect crystal at or near the exact angle for simultaneous *n*-beam diffraction through the crystal, 2*n* solutions of the complex dynamical diffraction equations exist for each angle of incidence. These give rise to 2*n* normal modes of propagation of X-rays. The real parts of the solutions determine the locations of 2*n* tiepoints, one on each sheet of the dispersion surface. The imaginary parts yield 2*n* absorption coefficients. At the incident surface, the boundary conditions determine the allocation of incident amplitude to each mode of propagation; at the exit surface they determine the distribution of the transmitted intensities among the diffracted beams.

The solution of the dynamical equations and the calculation of dynamical diffraction effects present formidable difficulties. Because of these difficulties, only a very few investigations in this area were undertaken in the years following the publication of Ewald's (1917) classic paper on the dynamical theory of X-ray diffraction. Interest in dynamical diffraction rose sharply following the discovery of the Borrmann effect (Borrmann, 1941). For many years, however, investigations of the effect were limited almost entirely to two-beam Bragg reflection or Laue transmission cases.

The situation changed following Borrmann & Hartwig's (1965) observation of a striking *additional* enhancement of the 111 reflection, anomalously transmitted through germanium, when the $11\bar{1}$ reflection is brought to diffracting position simultaneously with 111. Within a few years the results of large numbers of theoretical and experimental investigations of *n*-beam cases were published. These include: Saccocio & Zajac (1965), Hildebrandt (1967), Joko & Fukuhara (1967), Ewald & Heno (1968), Heno & Ewald (1968), Penning (1968), Uebach & Hildebrandt (1969), Balter, Feldman & Post (1971), Feldman & Post (1972), Huang & Post (1973), Hildebrandt (1973), Huang, Tillinger & Post (1973), Uebach (1973), Katsnelson, Iveronova, Borodina & Runova (1975).

Because of the complexity of the calculations, most of the above have been limited to *n*-beam effects which take place when the crystal is set at the exact angle for *n*-beam diffraction. The necessary calculations are then greatly simplified.

Diffraction limited to the exact *n*-beam setting implies a non-divergent incident beam. Real incident beams always possess finite divergence, and excite extensive portions of the dispersion surface of a stationary crystal. Transmitted 'peak' intensities are therefore actually integrated over finite angular ranges; the latter are determined mainly by the angular acceptance range of the crystal. Similarly, measured absorption coefficients represent values averaged over ranges of angles and, in many cases, over several modes of propagation. Analytic methods are not yet available for the calculation of such 'integrated' intensities, or averaged absorption coefficients, from data calculated for the *n*-beam point alone. To make possible meaningful comparisons with experimental results, it is therefore necessary that calculations of these and similar quantities be repeated for many crystal settings. These difficulties are compounded by the rapid variation of calculated values with small changes of crystal setting near the *n*-beam point.

* Supported in part by contract F44620-74-C-0065, US Army Joint Services to the Electronics Program and by NSF grant DMR 75-23680.

† Present address: Instituto de Fisica, Universidade Estadual de Campinas, Campinas, Sao Paulo, Brazil.

‡ IBM Research Laboratory, San Jose, California.

We have written computer programs, based on von Laue's (1960) modifications of the plane wave theory of Ewald (1917), for the calculation of diffraction effects for 'n' coplanar reciprocal lattice points, for any value of 'n', and for wide ranges of crystal settings. To illustrate the above we have selected a four-beam case involving the simultaneous transmission of X-rays through germanium crystals by the 000, $1\bar{1}1$, $3\bar{1}\bar{1}$ and $20\bar{2}$ reflections. This case has been discussed by Katsnelson, Kissin & Polyakova (1969) and Katnelson, Borodina & Kissin (1970), with somewhat confusing results. These authors treated it initially as a three-beam case involving only the relatively strong $1\bar{1}1$ and $20\bar{2}$ reflections. In a later publication, they recognized the four-beam nature of the interaction, but again did not include the $3\bar{1}\bar{1}$ contributions in their calculations, stating that the weak $3\bar{1}\bar{1}$ reflection could not significantly affect the n-beam calculations (Katsnelson, Iveronova, Borodina & Runova, 1972). In a more recent paper, (Katsnelson *et al.*, 1975), the results of some calculations based on four-beams were reported, but these differ significantly from those previously reported by the authors and from those we present below.

It should be clear that the 'weakness' of the two-beam intensity of a reflection does not necessarily imply that its contribution to an n-beam interaction ($n>2$) is negligible. This point is illustrated well in the three-beam case involving 000, 111, and $11\bar{1}$, (Borrmann & Hartwig, 1965), to which we referred above. At the three-beam point, that interaction results in the reduction of the minimum absorption coefficient from its two-beam value of 107 cm^{-1}, to less than 19 cm^{-1}. This reduction is accompanied by a spectacular enhancement of the transmitted intensity. Dynamical diffraction effects are invariant to permutations of indices of reflections. In the case referred to, 002 serves to 'couple' the 111 and $11\bar{1}$ reflections. The case could equally well be described as the 111, 002 case, with $11\bar{1}$ performing the coupling function. Obviously, the contributions of the 002 reflection to this three-beam interaction should not be ignored, even though its two-beam structure factor equals zero. Similar considerations apply to $3\bar{1}\bar{1}$ in the four-beam case, as will be demonstrated below.

In this paper we present an outline of n-beam theory and calculation procedures, results calculated for the four-beam case, and comparisons of the latter with experiment.

II. Theory

As pointed out by von Laue (1960) the calculation of n-beam dynamical X-ray effects involves the solution of Maxwell's equations for a medium with a periodic complex dielectric constant. A sum of plane waves in the form of a Bloch function, which satisfies Bragg's law and Maxwell's equations, is taken as the assumed solution for the crystal wave field:

$$\mathbf{D}=\sum_H \mathbf{D}_H \exp\left[-2\pi i(\mathbf{K}_H\,.\,\mathbf{r}-vt)\right] \tag{1}$$

$$\mathbf{D}=\exp\left[-2\pi i(\mathbf{K}_O\,.\,\mathbf{r}-vt)\right]\sum_H \mathbf{D}_H \exp\left(-2\pi i\mathbf{H}\,.\,\mathbf{r}\right). \tag{2}$$

$\mathbf{K}_H$ is the wave vector inside the crystal, directed towards the reciprocal lattice point H; $\mathbf{D}_H$ is the corresponding electric displacement vector, transverse to $\mathbf{K}_H$.

A set of mutually orthogonal unit vectors $\hat{\mathbf{K}}_H, \hat{\boldsymbol{\sigma}}_H, \hat{\boldsymbol{\pi}}_H$ is defined as follows: all $\hat{\boldsymbol{\pi}}$ vectors lie in or parallel to the plane of the 000, $1\bar{1}1$, $3\bar{1}\bar{1}$, $20\bar{2}$ reciprocal lattice points; also, $\mathbf{K}_H/|\mathbf{K}_H| = \hat{\boldsymbol{\sigma}}_H \times \hat{\boldsymbol{\pi}}_H$.

The solutions of Maxwell's equations lead to a set of linear, homogeneous equations for the wave field due to all the reciprocal lattice points ($O,H,P\ldots$) in diffracting positions, as follows (James, 1963):

$$2\varepsilon_H \mathbf{D}_H=\sum_P \varphi_{(H-P)}\mathbf{D}_{P(H)} \tag{3}$$

where

$$2\varepsilon_H=\frac{\mathbf{K}_H\,.\,\mathbf{K}_H}{k^2}-1\,, \tag{4}$$

$$\varphi_H=-\frac{e^2}{mc^2}\frac{\lambda^2}{\pi V}F_H\,, \tag{5}$$

$\mathbf{D}_{P(H)}$ is the vector component of $\mathbf{D}_P$ which is perpendicular to $\mathbf{K}_H$. $\mathbf{k}$ is the vacuum wave vector and V is the volume of the unit cell.

Equation (3) yields 'n' vector equations in an n-beam case. Each $\mathbf{D}_H$ can be decomposed into two

Table 1. *The eight scalar equations for a four-beam case*

$\hat{\boldsymbol{\sigma}}_O, \hat{\boldsymbol{\pi}}_O, \hat{\boldsymbol{\sigma}}_H, \hat{\boldsymbol{\pi}}_H, \ldots$ are unit vectors in the directions of $\mathbf{D}_O^{\sigma}, \mathbf{D}_O^{\pi}, \mathbf{D}_H^{\sigma}, \mathbf{D}_H^{\pi}, \ldots$.

$$\begin{bmatrix}
\varphi_O-2\varepsilon_O & \varphi_O\hat{\boldsymbol{\sigma}}_O\cdot\hat{\boldsymbol{\pi}}_O & \varphi_H\hat{\boldsymbol{\sigma}}_O\cdot\hat{\boldsymbol{\sigma}}_H & \varphi_H\hat{\boldsymbol{\sigma}}_O\cdot\hat{\boldsymbol{\pi}}_H & \varphi_P\hat{\boldsymbol{\sigma}}_O\cdot\hat{\boldsymbol{\sigma}}_P & \varphi_P\hat{\boldsymbol{\sigma}}_O\cdot\hat{\boldsymbol{\pi}}_P & \varphi_V\hat{\boldsymbol{\sigma}}_O\cdot\hat{\boldsymbol{\sigma}}_V & {}_V\hat{\boldsymbol{\sigma}}_O\cdot\hat{\boldsymbol{\pi}}_V \\
\varphi_O\hat{\boldsymbol{\pi}}_O\cdot\hat{\boldsymbol{\sigma}}_O & \varphi_O-2\varepsilon_O & \varphi_H\hat{\boldsymbol{\pi}}_O\cdot\hat{\boldsymbol{\sigma}}_H & \varphi_H\hat{\boldsymbol{\pi}}_O\cdot\hat{\boldsymbol{\pi}}_H & \varphi_P\hat{\boldsymbol{\pi}}_O\cdot\hat{\boldsymbol{\sigma}}_P & \varphi_P\hat{\boldsymbol{\pi}}_O\cdot\hat{\boldsymbol{\pi}}_P & \varphi_V\hat{\boldsymbol{\pi}}_O\cdot\hat{\boldsymbol{\sigma}}_V & {}_V\hat{\boldsymbol{\pi}}_O\cdot\hat{\boldsymbol{\pi}}_V \\
\varphi_H\hat{\boldsymbol{\sigma}}_H\cdot\hat{\boldsymbol{\sigma}}_O & . & \varphi_O-2\varepsilon_H & \varphi_O\hat{\boldsymbol{\sigma}}_H\cdot\hat{\boldsymbol{\pi}}_H & \varphi_{P-H}\hat{\boldsymbol{\sigma}}_H\cdot\hat{\boldsymbol{\sigma}}_P & \varphi_{P-H}\hat{\boldsymbol{\sigma}}_H\cdot\hat{\boldsymbol{\pi}}_P & \varphi_{V-H}\hat{\boldsymbol{\sigma}}_H\cdot\hat{\boldsymbol{\sigma}}_V & {}_{V-H}\hat{\boldsymbol{\sigma}}_H\cdot\hat{\boldsymbol{\pi}}_V \\
\varphi_H\hat{\boldsymbol{\pi}}_H\cdot\hat{\boldsymbol{\sigma}}_O & . & . & \varphi_O-2\varepsilon_H & \varphi_{P-H}\hat{\boldsymbol{\pi}}_H\cdot\hat{\boldsymbol{\sigma}}_P & \varphi_{P-H}\hat{\boldsymbol{\pi}}_H\cdot\hat{\boldsymbol{\pi}}_P & \varphi_{V-H}\hat{\boldsymbol{\pi}}_H\cdot\hat{\boldsymbol{\sigma}}_V & {}_{V-H}\hat{\boldsymbol{\pi}}_H\cdot\hat{\boldsymbol{\pi}}_V \\
\varphi_P\hat{\boldsymbol{\sigma}}_P\cdot\hat{\boldsymbol{\sigma}}_O & . & . & . & \varphi_O-2\varepsilon_P & \varphi_O\hat{\boldsymbol{\sigma}}_P\cdot\hat{\boldsymbol{\pi}}_P & \varphi_{V-P}\hat{\boldsymbol{\sigma}}_P\cdot\hat{\boldsymbol{\sigma}}_V & {}_{V-P}\hat{\boldsymbol{\sigma}}_P\cdot\hat{\boldsymbol{\pi}}_V \\
\varphi_P\hat{\boldsymbol{\pi}}_P\cdot\hat{\boldsymbol{\sigma}}_O & . & . & . & . & \varphi_O-2\varepsilon_P & \varphi_{V-P}\hat{\boldsymbol{\pi}}_P\cdot\hat{\boldsymbol{\sigma}}_V & {}_{V-P}\hat{\boldsymbol{\pi}}_P\cdot\hat{\boldsymbol{\pi}}_V \\
\varphi_V\hat{\boldsymbol{\sigma}}_V\cdot\hat{\boldsymbol{\sigma}}_O & . & . & . & . & . & \varphi_O-2\varepsilon_V & {}_O\hat{\boldsymbol{\sigma}}_V\cdot\hat{\boldsymbol{\pi}}_V \\
\varphi_V\hat{\boldsymbol{\pi}}_V\cdot\hat{\boldsymbol{\sigma}}_O & \varphi_V\hat{\boldsymbol{\pi}}_V\cdot\hat{\boldsymbol{\pi}}_O & \varphi_{H-V}\hat{\boldsymbol{\pi}}_V\cdot\hat{\boldsymbol{\sigma}}_H & \varphi_{H-V}\hat{\boldsymbol{\pi}}_V\cdot\hat{\boldsymbol{\pi}}_H & {}_{P-V}\hat{\boldsymbol{\pi}}_V\cdot\hat{\boldsymbol{\sigma}}_P\,. & \varphi_{P-V}\hat{\boldsymbol{\pi}}_V\cdot\hat{\boldsymbol{\pi}}_P & \varphi_O\hat{\boldsymbol{\pi}}_V\cdot\hat{a}_V & {}_O-2\varepsilon_H
\end{bmatrix}\cdot\begin{bmatrix}\varphi D_O^{\sigma}\\ \varphi D_O^{\pi}\\ \varphi D_H^{\sigma}\\ \varphi D_H^{\pi}\\ \varphi D_P^{\sigma}\\ \varphi D_P^{\pi}\\ \varphi D_V^{\sigma}\\ \varphi D_V^{\pi}\end{bmatrix}=0 \tag{6}$$

mutually orthogonal components, D_H^σ and D_H^π, to yield $2n$ scalar equations. For a four-beam case the eight scalar equations can be written as equation (6), shown in Table 1. The unknowns in (6) are the complex eigenvalues, ε_H, and the eigenvectors $\mathbf{D}_H^\sigma, \mathbf{D}_H^\pi, \cdots$ The real parts of the eigenvalues yield the positions of the tiepoints on the $2n$ sheets of the dispersion surface. The imaginary parts are proportional to the absorption coefficients.

The eigenvector solutions of (6) give the ratios of wave field amplitudes. The relative amounts of incident energy assigned to each mode of propagation are defined as follows:

$$\mathrm{Ex}_H(j)=\frac{|D_H^\sigma(j)|^2+|D_H^\pi(j)|^2}{|E_0^\sigma|^2+|E_0^\pi|^2}, \tag{7}$$

$\mathrm{Ex}_H(j)$ refers to the excitation of mode (j) in the beam directed to H. E_0^σ and E_0^π refer to the incident vacuum electric field components along the mutually perpendicular $\hat{\boldsymbol{\sigma}}$ and $\hat{\boldsymbol{\pi}}$ directions. For the four-beam case under consideration, the relations between the polarization vectors can be expressed in terms of $\theta_{3\bar{1}\bar{1}}$ and an angle, ψ, as follows:

$$\begin{aligned}
&\hat{\boldsymbol{\sigma}}_O\cdot\hat{\boldsymbol{\sigma}}_O=\hat{\boldsymbol{\pi}}_O\cdot\hat{\boldsymbol{\pi}}_O=\hat{\boldsymbol{\sigma}}_H\cdot\hat{\boldsymbol{\sigma}}_H=\hat{\boldsymbol{\pi}}_H\cdot\hat{\boldsymbol{\pi}}_H=\hat{\boldsymbol{\sigma}}_P\cdot\hat{\boldsymbol{\sigma}}_P=\hat{\boldsymbol{\pi}}_P\cdot\hat{\boldsymbol{\pi}}_P=\hat{\boldsymbol{\sigma}}_V\cdot\hat{\boldsymbol{\sigma}}_V=\hat{\boldsymbol{\pi}}_V\cdot\hat{\boldsymbol{\pi}}_V=1\\
&\hat{\boldsymbol{\sigma}}_O\cdot\hat{\boldsymbol{\pi}}_O=\hat{\boldsymbol{\sigma}}_H\cdot\hat{\boldsymbol{\pi}}_H=\hat{\boldsymbol{\sigma}}_P\cdot\hat{\boldsymbol{\pi}}_P=\hat{\boldsymbol{\sigma}}_V\cdot\hat{\boldsymbol{\pi}}_V=\hat{\boldsymbol{\pi}}_H\cdot\hat{\boldsymbol{\sigma}}_P=\hat{\boldsymbol{\sigma}}_H\cdot\hat{\boldsymbol{\pi}}_P=\hat{\boldsymbol{\pi}}_O\cdot\hat{\boldsymbol{\sigma}}_V=\hat{\boldsymbol{\sigma}}_O\cdot\hat{\boldsymbol{\pi}}_V=0\\
&\hat{\boldsymbol{\sigma}}_O\cdot\hat{\boldsymbol{\sigma}}_P=\hat{\boldsymbol{\sigma}}_H\cdot\hat{\boldsymbol{\sigma}}_V=\sin^2\theta_{(3\bar{1}\bar{1})}\cos^2\theta_{(3\bar{1}\bar{1})}\cos\psi\\
&\hat{\boldsymbol{\sigma}}_O\cdot\hat{\boldsymbol{\sigma}}_V=\hat{\boldsymbol{\sigma}}_H\cdot\hat{\boldsymbol{\sigma}}_P=\sin^2\theta_{(3\bar{1}\bar{1})}+\cos^2\theta_{(3\bar{1}\bar{1})}\cos\psi\\
&\hat{\boldsymbol{\sigma}}_H\cdot\hat{\boldsymbol{\sigma}}_V=\hat{\boldsymbol{\sigma}}_O\cdot\hat{\boldsymbol{\sigma}}_P=\sin^2\theta_{(3\bar{1}\bar{1})}-\cos^2\theta_{(3\bar{1}\bar{1})}\\
&\hat{\boldsymbol{\sigma}}_O\cdot\hat{\boldsymbol{\pi}}_H=\hat{\boldsymbol{\sigma}}_H\cdot\hat{\boldsymbol{\pi}}_V=\hat{\boldsymbol{\sigma}}_P\cdot\hat{\boldsymbol{\pi}}_O=\hat{\boldsymbol{\sigma}}_V\cdot\hat{\boldsymbol{\pi}}_H=\cos\theta_{(3\bar{1}\bar{1})}\sin\psi\\
&\hat{\boldsymbol{\sigma}}_O\cdot\hat{\boldsymbol{\pi}}_P=\hat{\boldsymbol{\sigma}}_H\cdot\hat{\boldsymbol{\pi}}_O=\hat{\boldsymbol{\sigma}}_P\cdot\hat{\boldsymbol{\pi}}_V=\hat{\boldsymbol{\sigma}}_V\cdot\hat{\boldsymbol{\pi}}_H=-\cos\theta_{(3\bar{1}\bar{1})}\sin\psi\\
&\hat{\boldsymbol{\pi}}_O\cdot\hat{\boldsymbol{\pi}}_H=\hat{\boldsymbol{\pi}}_P\cdot\hat{\boldsymbol{\pi}}_V=-\cos\psi\\
&\hat{\boldsymbol{\pi}}_O\cdot\hat{\boldsymbol{\pi}}_P=\hat{\boldsymbol{\pi}}_H\cdot\hat{\boldsymbol{\pi}}_V=\cos\psi\\
&\hat{\boldsymbol{\pi}}_O\cdot\hat{\boldsymbol{\pi}}_V=\hat{\boldsymbol{\pi}}_H\cdot\hat{\boldsymbol{\pi}}_P=-1
\end{aligned} \tag{8}$$

where O, H, P and V represent the 000, $1\bar{1}1$, $3\bar{1}\bar{1}$ and $20\bar{2}$ reciprocal lattice points. ψ equals $\tan^{-1}[d^*_{(1\bar{1}1)}/d^*_{(20\bar{2})}]$.

Since the wave solutions must satisfy the boundary conditions on the incident and exit surfaces of the crystal, the intensities of the transmitted beams can be calculated. For a crystal of thickness t the intensity of the diffracted beam, $I_H(t)$, at the exit surface is

$$I_H(t)=|\sum_j D_H(j)\exp[-2\pi i\mathbf{K}_H(j)\cdot\mathbf{r}]|^2 \tag{9}$$

where the summation is over the j modes of propagation $\mathbf{D}_H(j)=\hat{\boldsymbol{\sigma}}D^\sigma{}_H(j)+\hat{\boldsymbol{\pi}}D_H^\pi(j)$; $\hat{\boldsymbol{\sigma}}$ and $\hat{\boldsymbol{\pi}}$ are unit vectors, previously defined; and, $\mathbf{K}_H(j)=\mathbf{K}_H'(j)-i\mathbf{K}_H''(j)$. The latter two terms refer to the real and imaginary parts, respectively, of the jth mode of propagation of $\mathbf{K}_H$, the propagation vector. $\mathbf{r}$ is directed into the crystal in the direction of the surface normal. At the exit surface the magnitude of $\mathbf{r}$ equals the crystal thickness.

To a good approximation $\varepsilon\cong10^{-5}$, and from (4):

$$|\mathbf{K}_H|=k(1+\varepsilon_H) \tag{10}$$

$$|\mathbf{K}-i\mathbf{K}_H''|=k(1+\varepsilon_H'-i\varepsilon_H'') \tag{11}$$

$$\mathbf{K}_H''=k\varepsilon_H''. \tag{12}$$

From (9) we see that the intensity of reflection H equals:

$$I_H(t)=|\sum_j \mathbf{D}_H(j)[\exp-2\pi i\mathbf{K}_H''(j)\cdot\mathbf{r})]\times[\exp-2\pi\mathbf{K}_H''(j)\cdot\mathbf{r}]|^2. \tag{13}$$

III. Experimental

Our experimental procedures have been described previously (Huang & Post, 1973). A schematic diagram of the experimental arrangement is shown in Fig. 1. A divergent, unfiltered microbeam X-ray source and a speciment-to-film distance of 160 cm were used to record transmitted patterns with high resolution. The copper target had an effective size of 100×100 μm at a 4° take-off angle. The specimens were dislocation-free, parallel-sided germanium platelets, cut normal to [121]. The (000), $(1\bar{1}1)$, $(3\bar{1}\bar{1})$ and $(20\bar{2})$ reciprocal lattice points lie in a plane parallel to the crystal surface. All four points may be brought to their diffracting positions conveniently by rotating the crystal about [121] to bring $(3\bar{1}\bar{1})$ to the horizontal plane, and then tilting the crystal about the vertical axis to bring $(3\bar{1}\bar{1})$ to the surface of the Ewald sphere. The

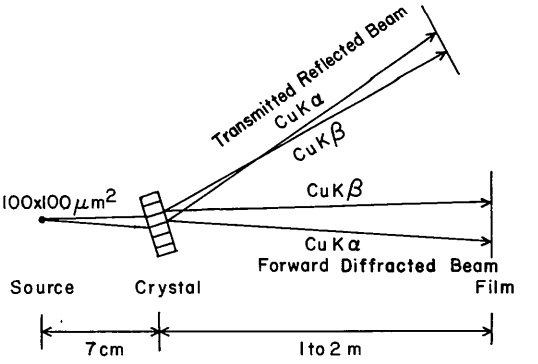

Fig. 1. Schematic drawing of the experimental arrangement.

crystal is aligned exactly for four-beam diffraction when the inward normal from the point where the incident beam strikes the crystal surface passes through the Laue point, L, (Fig. 2); L is equidistant, at a distance $1/\lambda_{(\text{vacuum})}$, from the reciprocal lattice points in their exact diffracting position.

In the lower part of Fig. 2 we show the plane of the four reciprocal lattice points. It is parallel to the surface of the crystal. The plane in the upper portion of the figure illustrates schematically the directions of the intersections of reflecting planes with a sheet of the dispersion surface. The intersections are referred to below as 'reflection lines'.

A transition from the four-beam case to one involving only two beams can be brought about by rotating the crystal about one of the three diffraction vectors shown in the lower part of Fig. 2. If, for example, the $[3\bar{1}\bar{1}]$ vector is horizontal, a change of the inclination of the incident beam which causes the point at which it impinges on the crystal surface to move in a vertical direction, is equivalent to a rotation of the crystal about $[3\bar{1}\bar{1}]$. The locus of the points of intersection of the incident beam with the crystal surface. coincides with the $3\bar{1}\bar{1}$ *reflection line, i.e.* with the line $M'M$. A transition from four beams to one occurs when the intersection of the incident beam with the surface moves in any direction other than along one of the reflection lines.

The use of a divergent incident beam eliminates the need for highly precise crystal alignment. The semi-apical angle of the cone of radiation incident on the crystal is about 4°, and photographs of the forward diffracted region will display the traces of the $1\bar{1}1$, $3\bar{1}\bar{1}$ and $20\bar{2}$ reflections, and their intersections, provided the crystal misalignment does not exceed 4°.

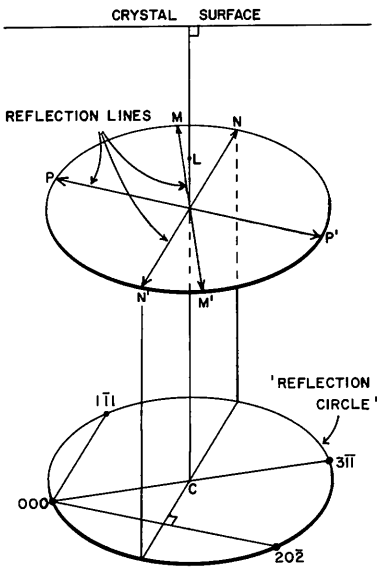

Fig. 2. The 'reflection circle' and 'reflection lines'.

The real and imaginary parts of the structure factors used in our calculations are listed in Table 2.

Table 2. *Structure factors of germanium*

The real parts were based on data listed in *International Tables for X-ray Crystallography* (1974); the imaginary parts were estimated from results published by Okkerse (1962). Corrections for thermal motion were applied using $B = 0{\cdot}556$ Å^2 (Okkerse, 1962).

hkl	$F'(hkl)$	$F''(hkl)$
000	245·60	7·345
1$\bar{1}$1	145·62	5·107
3$\bar{1}\bar{1}$	113·54	4·909
20$\bar{2}$	173·78	7·045

IV. Calculated results

Except where otherwise noted, the results listed in this section have been evaluated along reflection lines as functions of $\Delta\varphi$, the displacement from the four-beam point, at the following settings: $\Delta\varphi = 0$ to 24 seconds, at intervals of one second of arc, and at $\Delta\varphi = 32$, 64, 128 and 256 seconds.

(*a*) *The dispersion surface*

The intersections of the eight sheets of the dispersion surface with the planes formed by the line LC (Fig. 2) and each of the reflection lines, are shown in Fig. 3. The Laue point is at the origin. Ordinates are listed in cm^{-1}. The distance from the Laue point to the origin of the reciprocal lattice equals $1/\lambda_0$, *i.e.* about $6{\cdot}5 \times 10^7$ cm^{-1} for Cu $K\alpha$. The LC direction is vertical in Fig. 3. The traces of the two-beam reflection lines are horizontal. In the two-beam regions only four modes are excited; the traces of the corresponding sheets are marked by asterisks.

The maximum value of $\Delta\varphi$ in Fig. 3 is 16″. In the $20\bar{2}$ and $1\bar{1}1$ plots the separations of sheets 1 and 4 differ significantly from those of 5 and 8, on opposite sides of the four-beam point, at $|\Delta\varphi| = 16''$. Evidently, in these cases the transition from four to two beams is not complete at that setting. The gradual approach to 'equilibrium' two-beam $20\bar{2}$ conditions is illustrated in Table 3, in which we list distances between sheets of the dispersion surface at larger $\Delta\varphi$. At large $\Delta\varphi$, the separation of sheet 1 from 4 on one side of the four-beam point should be exactly equal to the corresponding separation of sheet 5 from 8 on the other side.

The individual values listed under A and B in Table 3 approach their asymptotic values very slowly; the *averaged* values, listed to the right, converge rapidly to an indicated separation of 1486 cm^{-1}. This value may be checked by making use of the known proportionality between the separations of sheets in two-beam regions and the magnitudes of the structure factors involved (Batterman & Cole, 1964), *i.e.*

$$S_H \cos\theta' = \frac{r_e\lambda}{\pi V}|P_H|\,|F_H|\,. \qquad (14)$$

r_e is the classical radius of the electron: $2{\cdot}818 \times 10^{-13}$ cm; V is the volume of the unit cell; S_H is the separation of sheets, in cm^{-1}; $|P_H|$ is the magnitude of the polarization factor; it equals unity for the two outer sheets (1 and 4, and 5 and 8), and cos 2θ for the inner sheets; θ' is the angle by which the plane of the reciprocal lattice points must be rotated from a position tangent to the Ewald sphere to bring the points to their simultaneous diffracting position. It equals the angle between LC (Fig. 2) and the line from L to one of the four reciprocal lattice points. For the four-beam case under study θ' equals 26·843°, the Bragg angle for diffraction by $(3\bar{1}\bar{1})$.

If we substitute the calculated value of 1486 cm^{-1} for S_H in (14), and take $|P|=1$, we obtain $|F_H|=173{\cdot}77$, in good agreement with the 173·78 initially assumed for our calculations. Similarly, the substitution of the calculated value of 1045 cm^{-1} for the separation of the two inner sheets, and using $\theta_{\text{Bragg } 20\bar{2}}$ (22·6485°) to calculate the polarization factor, yields $|F_H|=173{\cdot}72$.

(*b*) *Relative excitations*

The relative excitations of the modes of propagation, calculated according to (7), are shown in Fig. 4. Closely spaced pairs of lines have been combined in some cases to minimize confusion.

Examination of Figs. 3 and 4 indicates that the arrangements of sheets of the dispersion surface are of two types. Along $1\bar{1}1$ and $20\bar{2}$, on one side of the $\Delta\varphi=0$ setting, one set of four sheets is excited in the two-beam region; on the other side it is replaced by another set of four. Near the four-beam point (*i.e.* along $\Delta\varphi=0$), both sets are excited to provide the eight modes needed for four-beam cases. In the second arrangement, (along $3\bar{1}\bar{1}$), modes 3,4,5 and 6 are excited on *both* sides of the four-beam point. Near $\Delta\varphi=0$, four additional modes are excited (1 and 2, and 7 and 8). This arrangement shows almost perfect mirror symmetry across $\Delta\varphi=0$ [Figs. 3(*c*) and 4(*c*)].

Table 3. *Separations of sheets along the* $20\bar{2}$ *line* (*in* cm^{-1})

$\Delta\varphi$ (seconds)	A 1 to 4	B 5 to 8	$(A+B)/2$
16	1803	1157	1480
32	1659	1311	1485
64	1575	1396	1485·5
128	1530	1441	1485·5
256	1509	1463	1486

The difference between the two arrangements appears to reflect the difference between the effects of rotation about $[1\bar{1}1]$ or $[20\bar{2}]$ from rotation about $[3\bar{1}\bar{1}]$. Rotation about either of the first two diffraction vectors through $\Delta\varphi=0$ results in the simultaneous movement of two reciprocal lattice points either *into or out of* the Ewald sphere (see Fig. 2). A similar rotation about $[3\bar{1}\bar{1}]$ causes the $(1\bar{1}1)$ and $(20\bar{2})$ reciprocal lattice points, which are symmetrically arranged about [311], to move in *opposite* directions through the sphere.

The coordinates of the dispersion surface are determined by the real parts of ε_H, the 'resonance error', defined in (4). The overall resonance error should be almost independent of rotation through the four-beam point when the rotation axis is $[3\bar{1}\bar{1}]$; it should change by large amounts, asymmetrically, when the crystal is rotated about either $[1\bar{1}1]$ or $[20\bar{2}]$.

The excitation curves along $1\bar{1}1$ and $20\bar{2}$ vary irregularly near the four-beam point. The corresponding absorption curves are, however, symmetrical across $\Delta\varphi=0$, and it is clear that in those cases any asymmetry of the transmitted intensities must be due to the asymmetry of the corresponding excitations [see § IV(*d*)].

(*c*) *Absorption coefficients*

The absorption coefficients of the eight modes, along the three reflection lines, are shown in Fig. 5. At the

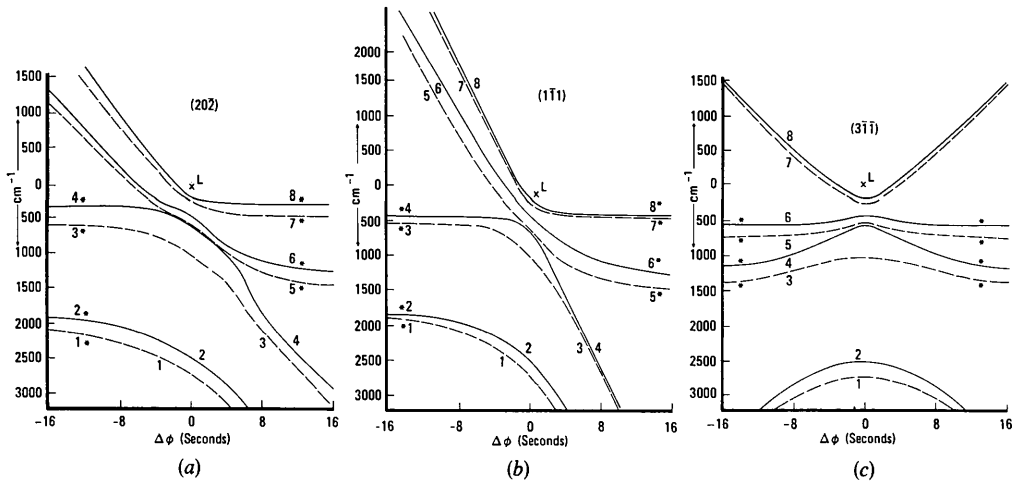

Fig. 3. Sections through the four-beam dispersion surface.

four-beam point, the minimum value is 6·2 cm^{-1}, compared with the one-beam coefficient of 352 cm^{-1}, or with the minimum two-beam values of 14·4, 107·3 and 116·8 cm^{-1} for $20\bar{2}$, $1\bar{1}1$ and $3\bar{1}\bar{1}$ respectively. A convenient check on the validity of these calculations is based on the numerical equality that exists between the sum of the eigenvalues and the trace of a matrix (Noble, 1969). It follows that the sum of the imaginary eigenvalues of (6) $[\Sigma_j \varepsilon''(j)]$ should be constant and should equal $2\pi R\varphi_0''$ at *all* crystal settings. The latter is equal to the average macroscopic absorption coefficient, μ_0, (Zachariasen, 1945).

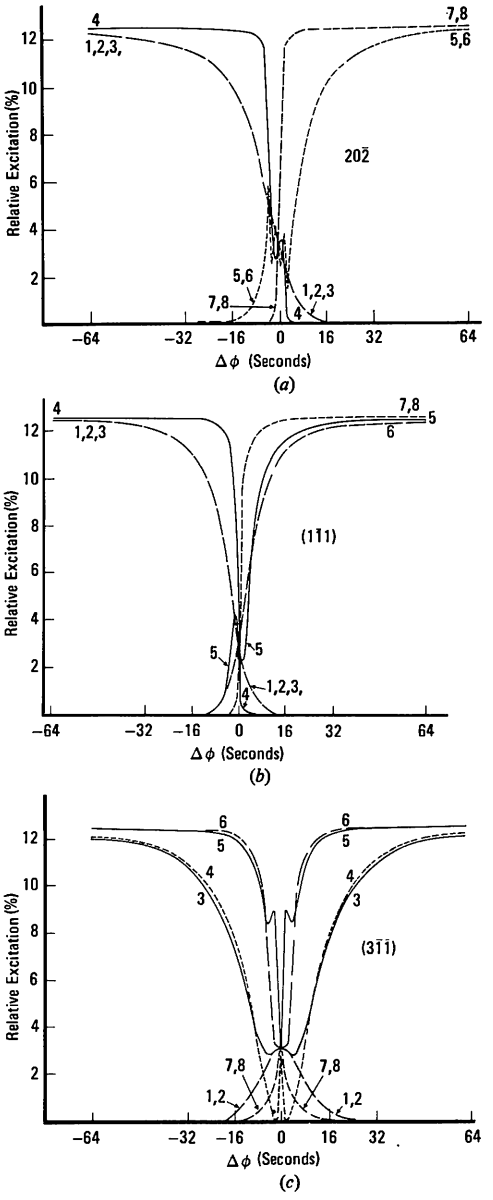

Fig. 4. Excitations of modes of propagation.

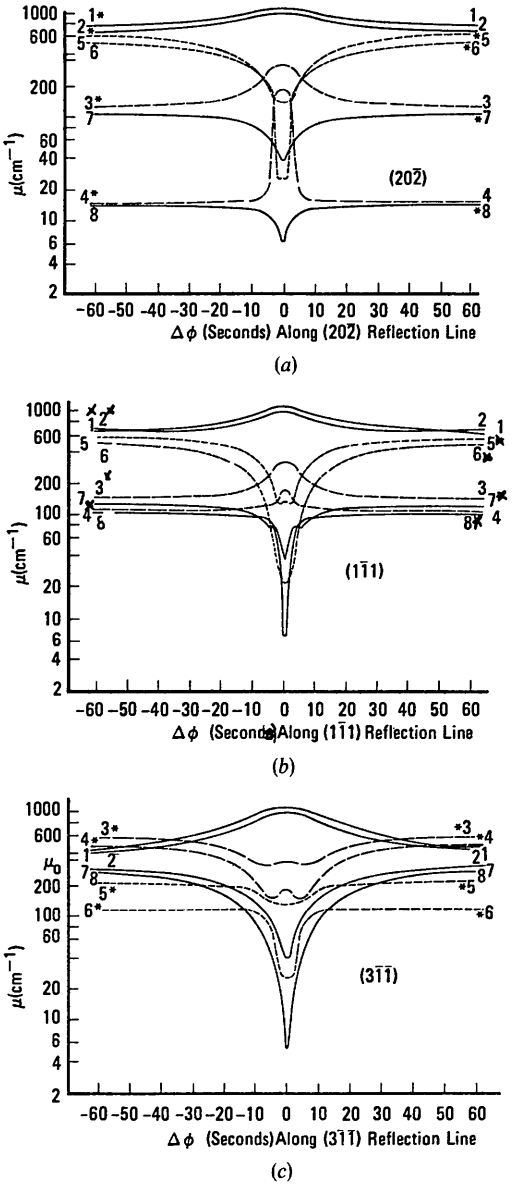

Fig. 5. Two and four-beam absorption coefficients.

Table 4. *Average absorption coefficients of modes 'active' in two-beam regions near a four-beam point* (*in* cm^{-1})

	Reflection line		
$\Delta\varphi$ (seconds)	$1\bar{1}1$	$3\bar{1}\bar{1}$	$20\bar{2}$
128	336·9	349·8	332·1
300	345·6	351·7	343·6
600	348·9	352·0	347·8

In two-beam regions only four modes are excited; the *average* of the four 'effective' coefficients should therefore also equal μ_0. Differences between the two, in regions distant from the *n*-beam point, indicate the persistence of the effects of the *n*-beam interaction. Some such differences are listed in Table 4.

The data in Table 4 apply to regions of positive

$\Delta\varphi$. Discrepancies of opposite sign are found along reflection lines in the corresponding regions of negative $\Delta\varphi$. Similar effects occur in one-beam regions. The averages of the two effective absorption coefficients along a line perpendicular to $3\bar{1}\bar{1}$ are only 318·9, 335·1 and 342·9 cm^{-1} at $\Delta\varphi = 150$, 300 and 600 seconds. These long-range effects indicate the need for caution in interpreting the results of absorption measurements in perfect crystals, particularly when short-wavelength radiations are used. The number of n-beam interactions increases as the inverse cube of the wavelength and the difficulty of locating crystal settings free from such effects varies correspondingly.

(d) Transmitted intensities

The relative intensities (I/I_0) of the diffracted beams have been calculated, using (13), for settings along each reflection line at angular intervals of one second of arc to $\Delta\varphi = 30''$. Results for thicknesses of 0·0025, 0·05 and 0·1 cm are shown in Fig. 6.

The 'forward diffracted' and 'transmitted reflected' beam intensities (defined in Fig. 1) oscillate widely in the thin crystal cases ($t = 0{\cdot}0025$ cm). In these, all modes may contribute to the diffracted intensities. The sum indicated by (13) involves positive, squared terms, as well as cross-terms which may be either positive or negative. In thin crystals the cross-terms are comparable in magnitude to the squared terms: hence the oscillatory behavior. As the crystal thickness increases, the high absorption modes are preferentially attenuated; in most cases of moderately 'thick' crystals, only one or two modes make appreciable contributions to the intensities. The intensity curves become progressively smoother with increasing thickness as shown in Fig. 6.

The following intensity anomalies should be noted: along $3\bar{1}\bar{1}$ and $1\bar{1}1$ the intensity at the four-beam point is strongly enhanced; enhancement is minor along $20\bar{2}$; abrupt decreases in intensity occur along $20\bar{2}$ and $1\bar{1}1$ near the four-beam point. These will be compared with experimental results.

(e) Weak reflections

In the *Introduction* we referred to n-beam calculations from which the contributions of 'weak reflections' had been omitted. Such omissions are common and sometimes justified in electron diffraction calculations, where n-beam interactions may involve very large numbers of reflections. In X-ray dynamical calculations they are clearly unjustified, at least in the three-beam case which we cited. To illustrate the corresponding effect in our four-beam case, we have calculated values of the absorption coefficients and the excitations of modes, for the exact n-beam point, both for an 'artificial' three-beam case from which the $3\bar{1}\bar{1}$ contributions were omitted, and for one involving all four beams. These are listed in Table 5, from which it should be evident that the omission of the contributions of weak (two-beam) reflections from n-beam calculations may lead to serious errors in the calculated results.

V. Experimental results

Photographs of the four-beam forward diffracted and transmitted diffracted regions of reciprocal space are shown in Figs. 7 and 8. The specimen was an essentially perfect [121] cut germanium wafer about 0·5 mm thick.

In interpreting these photographs it is necessary to take into account the divergent and polychromatic na-

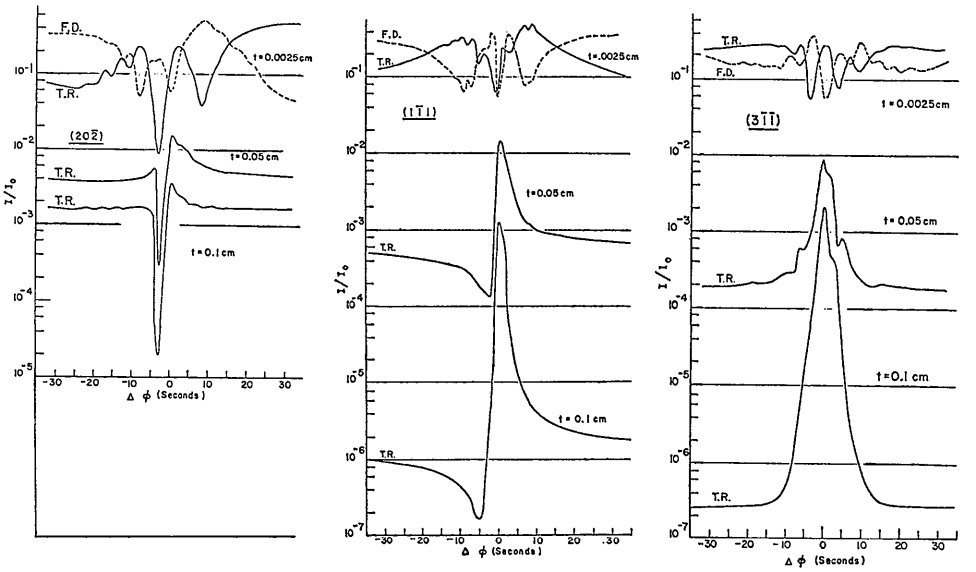

Fig. 6. Transmitted intensities, calculated. (F.D. = 'forward diffracted'; T.R. = 'transmitted reflected').

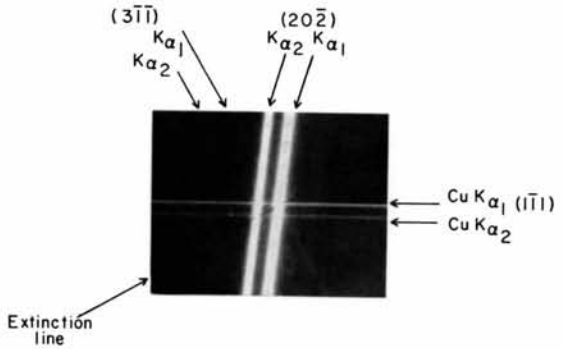

Fig. 7. Forward diffracted beams, experimental.

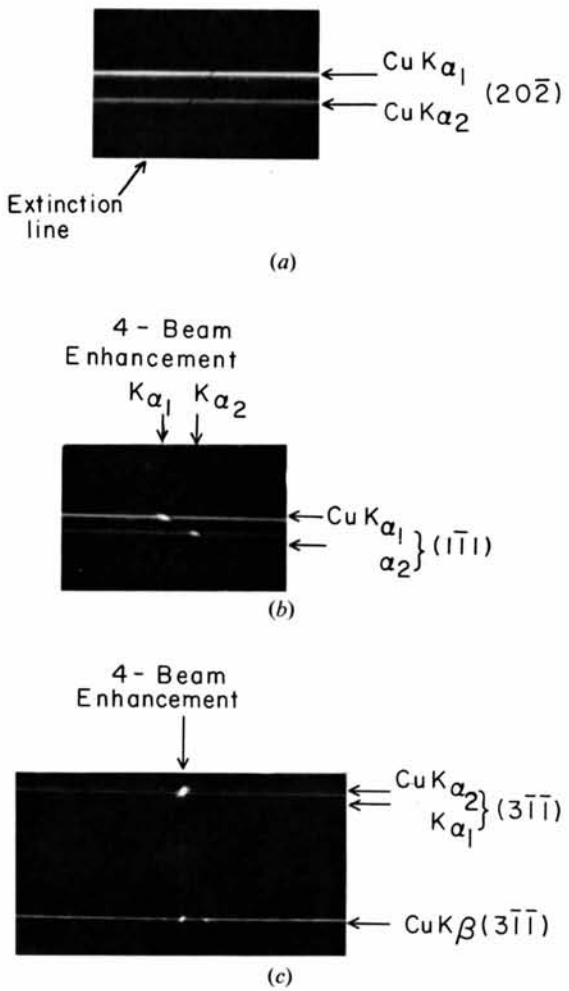

Fig. 8. Transmitted reflected beams. (*a*) 20$\bar{2}$, (*b*) 1$\bar{1}$1, (*c*) 3$\bar{1}\bar{1}$.

[*To face p.* 97

Table 5. *Effects of omission of a weak reflection from four-beam calculations*

Modes	Absorption coefficients (cm^{-1}) (at n-beam point) Four beams	'Three beams'	Excitations (%) Four beams	'Three beams'
1	6·2	20	12·5	28·6
2	37	77	12·5	28·5
3	25	132	12·5	1·1
4	133	234	12·5	2·4
5	177	776	12·5	20·5
6	324	875	12·5	18·8
7	1000		12·5	
8	1115		12·5	

ture of the incident Cu K beam. The divergence is approximately 4° in all directions. All wavelengths which satisfy the diffraction conditions for the 'n' reflections contribute to the recorded intensities. The diffraction lines recorded on the photographs are actually small, curved portions of Kossel conic sections, greatly magnified by the large specimen to film distance.

V(a) Forward diffracted beams (Fig. 7)

Four-beam points lie at the intersections of the diffraction lines due to *all* the radiations, continuous as well as characteristic, which are simultaneously diffracted by $(20\bar{2})$, $(1\bar{1}1)$ and $(3\bar{1}\bar{1})$. The most intense lines are due to diffraction of Cu $K\alpha_1$ and $K\alpha_2$ by $(20\bar{2})$ and $(1\bar{1}1)$. Near their intersections a faint 'extinction' line may be observed along the direction perpendicular to the $3\bar{1}\bar{1}$ line. It is shown enlarged in Fig. 7. The extinction line corresponds to the sharp dips in the $20\bar{2}$ and $1\bar{1}1$ transmitted intensities near the four-beam point; the dips affect all diffracted wavelengths: hence the extinction *line*. On the original films the extinction could be easily seen at the Cu $K\beta$ intersection as well.

V(b) Transmitted reflected beams

The effects of the four-beam interaction on the three transmitted reflection lines are shown in Fig. 8. A sharp discontinuity in the $20\bar{2}$ $K\alpha_1$ and α_2 lines (indicated by arrows) is clearly visible; it corresponds to the intensity dip shown along $20\bar{2}$ in Fig. 6. A very slight enhancement of the $20\bar{2}$ diffraction lines is detectable (with some effort) immediately adjacent to the discontinuities. The $1\bar{1}1$ photograph shows considerable enhancement of the transmitted beam adjacent to and partly overlapping a discontinuity in the diffraction line. The intensity of the $3\bar{1}\bar{1}$ reflection is even more strongly enhanced at the four-beam point, but there is no evidence of any intensity discontinuity or decrease nearby.

A faint line may be observed perpendicular to $3\bar{1}\bar{1}$ connecting the $K\alpha_1$ and α_2 lines with the $K\beta$ line. Diffraction of the continuum of non-characteristic wavelengths by $(3\bar{1}\bar{1})$ cannot lead to the appearance of reflection 'lines' on photographs. Such two-beam diffraction contributes only to the general background. At the four-beam points for these wavelengths, however, the transmitted intensities are greatly enhanced, giving rise to the line under discussion.

Agreement between the calculated results shown in Fig. 6 and those recorded photographically is generally satisfactory. All the intensity anomalies displayed in Fig. 6 are observed with approximately the indicated magnitudes. Even the slight deviation of the extinction line from the exact four-beam crossover point, which is indicated by the locations of the intensity dips on the $1\bar{1}1$ and $20\bar{2}$ charts (Fig. 6), is clearly visible on Fig. 7.

It is evident that classical dynamical diffraction theory can serve as the basis for reasonably accurate calculations of four-beam diffraction effects.

References

BALTER, S., FELDMAN, R. & POST, B. (1971). *Phys. Rev. Lett.* **27**, 307–309.

BATTERMAN, R. & COLE, H. (1964). *Rev. Mod. Phys.* **36**, 681–717.

BORRMANN, G. (1941). *Phys. Z.* **42**, 157–162.

BORRMANN, G. & HARTWIG, W. (1965). *Z. Kristallogr.* **121**, 401–409.

DALISA, A., ZAJZC, A. & NG, C. H. (1968). *Phys. Rev.* **168**, 854–858.

EWALD, P. P. (1917). *Ann. Phys. (Leipzig)*, **54**, 519–556; 557–597.

EWALD, P. P. & HENO, Y. (1968). *Acta Cryst.* A**24**, 5–15.

FELDMAN, R. & POST, B. (1972). *Phys. Stat. Sol.* **12**, 273–276.

HENO, Y. & EWALD, P. P. (1968). *Acta Cryst.* A**24**, 16–42.

HILDEBRANDT, G. (1967). *Phys. Stat. Sol.* **24**, 245–261.

HILDEBRANDT, G. (1973). *Phys. Stat. Sol.* A**15**, K83-86.

HUANG, T. C. & POST, B. (1973). *Acta Cryst.* A**29**, 35–37.

HUANG, T. C., TILLINGER, M. H. & POST, B. (1973). *Z. Naturforsch.* **28a**, 600–603.

International Tables for X-ray Crystallography (1974). Vol. IV. Birmingham: Kynoch Press.

JAMES, R. W. (1963). *Solid State Phys.* **15**, 53–220.

JOKO, T. & FUKUHARA, A. (1967). *J. Phys. Soc. Japan*, **22**, 597–604.

KATSNELSON, A. A., BORODINA, I. I. & KISSIN, V. I. (1970). *Phys. Stat. Sol. (A)*, **3**, 105–110.

KATSNELSON, A. A., IVERONOVA, V. I., BORODINA, T. I. & RUNOVA, T. K. (1975). *Phys. Stat. Sol. (A)*, **28**, 365–370.

KATSNELSON, A. A., IVERONOVA, V. I., BORODINA, T. I. & SAPKOVA, I. G. (1972). *Phys. Stat. Sol. (A)*, **11**, 39–44.

KATSNELSON, A. A., KISSIN, V. I. & POLYAKOVA, N. A. (1969). *Sov. Phys. Crystallogr.* **14**, 965–970.

LAUE, M. VON (1960). *Rontgenstrahl-Interferenzen.* Frankfurt am Main: Akademische Verlag.

NOBLE, B. (1969). *Applied Linear Algebra*, p. 280. New York: Prentice Hall.

OKKERSE, B. (1962). *Philips Res. Rep.* **17**, 464–478.

PENNING, P. (1968). *Philips Res. Rep.* **23**, 1–11; 12–24.

SACCOCIO, E. J. & ZAJAC, A. (1965). *Acta Cryst.* **18**, 478–480.

UEBACH, W. (1973). *Z. Naturforsch.* **28a**, 1214–1220.

UEBACH, W. & HILDEBRANDT, G. (1969). *Z. Kristallogr.* **129**, 1–8.

ZACHARIASEN, W. H. (1945). *Theory of X-ray Diffraction in Crystals.* New York: Dover.